An extended abstract for Heat Transfer in Nuclear Systems, 9th AIAA/ASME Joint Thermophysics and Heat Transfer Conference, San Francisco, CA, 5-8 June 2006

Analysis of Material Sample Heated by Impinging Hot Hydrogen Jet in a Non-Nuclear Tester

Ten-See Wang*, John Foote, and Ron Litchford
NASA Marshall Space Flight Center, Huntsville, Alabama, 35812

A computational conjugate heat transfer methodology was developed and anchored with data obtained from a hot-hydrogen jet heated, non-nuclear materials tester, as a first step towards developing an efficient and accurate multiphysics, thermo-fluid computational methodology to predict environments for hypothetical solid-core, nuclear thermal engine thrust chamber. The computational methodology is based on a multidimensional, finite-volume, turbulent, chemically reacting, thermally radiating, unstructured-grid, and pressure-based formulation. The multiphysics invoked in this study include hydrogen dissociation kinetics and thermodynamics, turbulent flow, convective and thermal radiative, and conjugate heat transfers. Predicted hot hydrogen jet and material surface temperatures were compared with those of measurement. Predicted solid temperatures were compared with those obtained with a standard heat transfer code. The interrogation of physics revealed that reactions of hydrogen dissociation and recombination are highly correlated with local temperature and are necessary for accurate prediction of the hot-hydrogen jet temperature.

I. Introduction

Nuclear thermal propulsion (NTP) may open up the solar system to far broader and faster exploration than is now possible with chemical propulsion. The feasibility of NTP systems was established by extensive testing in the Rover/NERVA programs and the technical merits of NTP have been identified and summarized.[1] The heat transfer efficiency and degree of hydrogen dissociation are two important performance factors for NTP. On the other hand, the need to push fuel element temperature to extremes in order to maximize performance also intensifies hydrogen induced corrosion rates, which are known to increase in direct proportion to reactor operating temperature.[2] In order to develop candidate high temperature fuel materials that would be compatible with the hot-hydrogen environment of a high performance solid core NTP engine, a non-nuclear test effort entitled "Hot Hydrogen Materials and Component Development" is underway at NASA's Marshall Space Flight Center (MSFC), while a parallel task entitled "Multiphysics Thrust Chamber Modeling" is also in progress in order to develop a computational methodology capable of predicting the thermal-fluid environment in a nuclear thermal engine thrust chamber. This computational methodology is based on an Unstructured-grid Navier-Stokes Internal-external computational fluid dynamics (CFD) Code (UNIC). Physical and numerical models pertinent to solid-core NTP will be developed and implemented. In this effort, as a first step, the hot gas and material temperatures to be measured in the hot-hydrogen materials development tests will be used to benchmark the UNIC code, while the computed solid temperatures will be compared with those obtained from a standard heat transfer code. The physics invoked in heating the materials with an impinging hot hydrogen jet are discussed and factors that may reduce the thermal gradient in the materials are investigated.

II. Computational Methodology

A. Computational Fluid Dynamics

*Technical Assistant, ER43, Thermal and Combustion Analysis Branch, Propulsion Structure, Thermal, and Fluids Analysis Division, Senior Member AIAA.

The CFD methodology is based on a multi-dimensional, finite-volume, viscous, chemically reacting, unstructured grid, and pressure-based formulation. Time-varying transport equations of continuity, species continuity, momentum, total enthalpy, turbulent kinetic energy, and turbulent kinetic energy dissipation were solved using a time-marching sub-iteration scheme and are written as:

$$\frac{\partial \rho}{\partial t}+\frac{\partial}{\partial x_j}\left(\rho u_j\right)=0 \tag{1}$$

$$\frac{\partial \rho \alpha_i}{\partial t}+\frac{\partial}{\partial x_j}\left(\rho u_j \alpha_j\right)=\frac{\partial}{\partial x_j}\left[\left(\rho D+\frac{\mu_t}{\sigma_\alpha}\right)\frac{\partial \alpha_i}{\partial x_j}\right]+\omega_i \tag{2}$$

$$\frac{\partial \rho u_i}{\partial t}+\frac{\partial}{\partial x_j}\left(\rho u_j u_i\right)=-\frac{\partial p}{\partial x_i}+\frac{\partial \tau_{ij}}{\partial x_j} \tag{3}$$

$$\frac{\partial \rho H}{\partial t}+\frac{\partial}{\partial x_j}\left(\rho u_j H\right)=\frac{\partial p}{\partial t}+Q_r+\frac{\partial}{\partial x_j}\left(\left(\frac{K}{C_p}+\frac{\mu_t}{\sigma_H}\right)\nabla H\right)+\frac{\partial}{\partial x_j}\left(\left((\mu+\mu_t)-\left(\frac{K}{C_p}+\frac{\mu_t}{\sigma_H}\right)\right)\nabla\left(V^2/2\right)\right)+\theta \tag{4}$$

$$\frac{\partial \rho k}{\partial t}+\frac{\partial}{\partial x_j}\left(\rho u_j k\right)=\frac{\partial}{\partial x_j}\left[\left(\mu+\frac{\mu_t}{\sigma_k}\right)\frac{\partial k}{\partial x_j}\right]+\rho(\Pi-\varepsilon) \tag{5}$$

$$\frac{\partial \rho \varepsilon}{\partial t}+\frac{\partial}{\partial x_j}\left(\rho u_j \varepsilon\right)=\frac{\partial}{\partial x_j}\left[\left(\mu+\frac{\mu_t}{\sigma_\varepsilon}\right)\frac{\partial \varepsilon}{\partial x_j}\right]+\rho\frac{\varepsilon}{k}\left(C_1\Pi-C_2\varepsilon+C_3\Pi^2/\varepsilon\right) \tag{6}$$

A predictor and corrector solution algorithm was employed to provide coupling of the governing equations. A second-order central-difference scheme was employed to discretize the diffusion fluxes and source terms. For the convective terms, a second-order upwind total variation diminishing difference scheme was used. To enhance the temporal accuracy, a second-order backward difference scheme was employed to discretize the temporal terms. Details of the numerical algorithm can be found in Ref's 3-7.

An extended k-ε turbulence model[8] was used to describe the turbulence. A modified wall function approach was employed to provide wall boundary layer solutions that are less sensitive to the near-wall grid spacing. Consequently, the model has combined the advantages of both the integrated-to-the-wall approach and the conventional law-of-the-wall approach by incorporating a complete velocity profile and a universal temperature profile[6]. A 2-species, 3-reaction detailed mechanism[9] was used to describe the hydrogen dissociation and recombination chemical kinetics.

B. Computational Conjugate Heat Transfer in Solids

The solid heat conduction equation is solved with the gas-side heat flux distributions as its boundary conditions. The solid heat conduction equation can be written as:

$$\frac{\partial \rho C T}{\partial t}-\frac{\partial}{\partial x_i}\left(\kappa\frac{\partial T}{\partial x_i}\right)=Q_v+Q_s \tag{7}$$

where Q_v and Q_s represent source terms from volumetric and boundary contributions, respectively. κ and C denote the thermal conductivity and capacity of the solid material, respectively. The temperature value at the gas-solid interface is obtained by enforcing the heat flux conservation condition. The boundary heat flux is,

$$q_w=\left(\kappa\frac{dT}{dx}\right)_b \quad \text{where } q_w \text{ is the heat flux from the fluid side.} \tag{8}$$

Numerically, it is expressed as:

$$q_w = \kappa \frac{T_c - T_b}{y_n}$$

$$\text{or} \quad T_b = T_c - \frac{q_w y_n}{\kappa} \tag{9}$$

where y_n represent the normal distance from the boundary to the center of the solid cell next to the boundary, T_c is the temperature at the center of the solid cell and T_b is the temperature at the interface boundary. The source term for the cell is then calculated as:

$$Q_s = \kappa \frac{T_b - T_c}{y_n} \tag{10}$$

To avoid numerical oscillations, an under-relaxation parameter is assign when evaluating the boundary temperature from Eq. (9). This step affects the source term accuracy using Eq. (10). Also, the source term calculated from (10) can be very large when a case is started, depending of the initial condition specified. This also contributed to numerical instability in the solution procedure. To fix this problem, the source term, Eq. (10), is separated into an explicit and an implicit parts. This source term linearization modification makes the solution procedure stable even for very large boundary heat fluxes. They are,

$$(Q_s)_e = \kappa \frac{T_b}{y_n} \tag{11}$$

$$(Q_s)_i = -\kappa \frac{T_c}{y_n} \tag{12}$$

The explicit source is added to the right-hand-side of the heat conduction equation while the implicit source term contributes to the diagonal terms of the final system of linear algebra equations.

III. Test Fixture Description

The test apparatus for testing tubular fuel materials is shown in Fig. 1. It is directly mated to an arc-heater (not shown) that provides hot-hydrogen flow. Optical ports are fitted to allow real-time pyrometer and laser diagnostics measurements for material surface temperature and centerline gas temperature, respectively. As the hot-hydrogen jet travels the length of the chamber, it loses energy to the water-cooled copper chamber and sample material. As the sample material heats up, it loses energy to the colder chamber wall by thermal radiation. A shield serving as both convective and radiative shielding was added through a detailed design analyses, resulting in minimum heat load on the water-cooled copper chamber wall and maximum hot hydrogen delivering temperature.

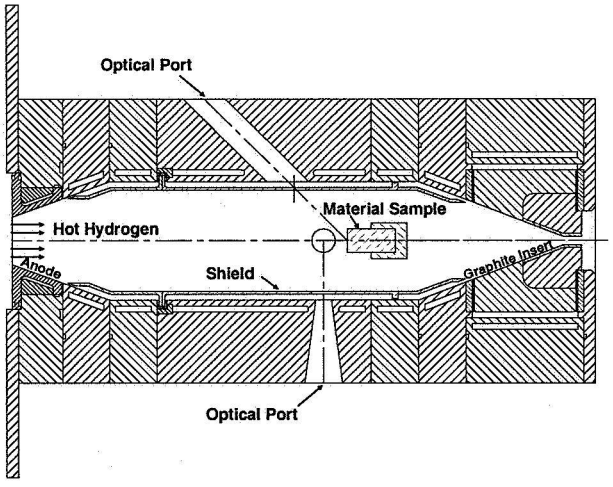

Fig 1. Test apparatus.

IV. Computational Grid Generation

Hybrid computational grids were generated using a software package GRIDGEN. A series of grid verification studies were performed to determine the current grid size. It was also found during the grid study that the computed gas-solid interface temperature is most stable when structured-grid layers are present on both sides of the interface.

V. Boundary Conditions

No-slip condition was applied to the solid walls. Fixed mass flow rate boundary condition was used at the inlet, and mass conservation boundary condition was used at the exit. For a conservative calculation of the chamber wall heat flux, a fixed temperature of 400 K was estimated for the chamber wall and the hot-hydrogen temperature was set at 3500 K. The wall temperature of the shield facing the chamber wall was estimated to be 2600 K from a separate one-dimensional heat transfer calculation. Adiabatic condition was applied to walls of opposing-side shield and flanges, and graphite insert (the convergent section). The hydrogen inlet mass flow rate was 10 g/s and the chamber pressure was 35 atm. An emissivity of 0.6 was applied to the copper chamber wall, whereas an emissivity of 0.4 was applied to the shield. The emissivity for the rest of the solid walls was set at 0.9. The inlet boundary was considered as a radiating wall to approximate the radiation from the arc-heater section. A series of pre-calculations were performed to iterate the inlet temperature and species concentrations such that the inlet species concentrations correspond to a state of temperature at 3500 K.

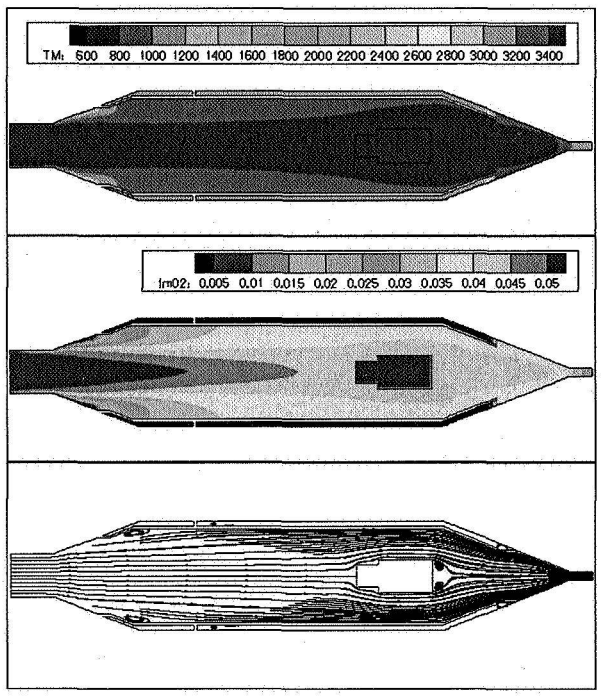

Fig. 2 From top to bottom, computed temperature and H Mass Fraction Contours and Streamlines.

VI. Results and Discussion

Figure 2 shows typical computed temperature, H concentration contours and streamlines under normal test conditions. It can be seen from the temperature contours that the entire thrust chamber is almost uniformly heated, except for the region between the shield and the cooled chamber wall. This is because the shield serves as both convection and radiation shields. Nevertheless, the hot hydrogen jet loses energy as it heats up the sample. When that happens, H recombines to become H_2. This is shown in the H contours where its concentration decreases as the hot jet approaches the sample. The streamlines show an expanding hot-hydrogen jet impinging on and flowing around the sample coupon, and later exhausting into the convergent exit section. A large recirculation zone appears in the divergent section of the chamber, while a small recirculation region forms behind the sample holder; both of which are strongly affected by the turbulence. Note although the plots in Fig. 2 showing a distinctive strong hot-hydrogen jet and two recirculated flow regions, the pressure and Mach number contours are fairly uniform inside the chamber (not shown), due to the largely low subsonic flow field and the protection of the shield. The integrity of the sample being heated by such a high temperature environment is the subject of the test.

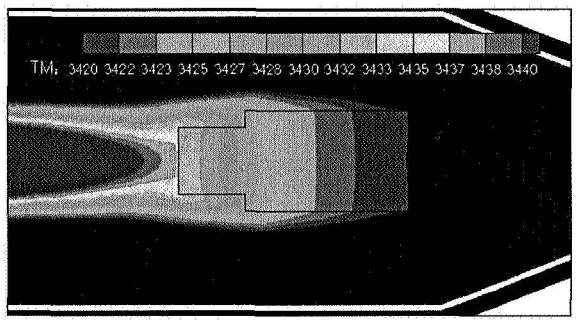

Figure 3 shows typical temperature contours surrounding and inside the sample coupon. It can be seen that heat is being transferred from the impinging hot hydrogen jet to the sample coupon. For different materials with different thermal properties, the thermal gradient inside the sample coupon will be different. The computed temperature contours inside the sample coupon appears to be reasonable.

VII. Summary

A computational conjugate heat transfer methodology was developed, to study the effect of hot hydrogen jet impinging on sample coupon made of different materials. The computational result of check out runs appears to be reasonable. A series of tests are scheduled from November to December. The test results will be used to benchmark the computational methodology. The computational methodology will then be used to perform parametric studies to assess factors that might reduce thermal gradient inside the sample material.

Acknowledgments

This study was partially supported by a Nuclear Systems Office task entitled "Multiphysics Thrust Chamber Modeling" and by a MSFC Internal Research and Development focus area task entitled "Hot-Hydrogen Materials and Component Development."

References

[1]Koenig, D.R., "Experience Gained from the Space Nuclear Rocket Program (Rover)," LA-10062-H, Los Alamos National Laboratory, Los Alamos, New Mexico, 1986.

[2]Lyon, L.L., "Performance of (U,Zr)C-Graphite (Composite) and of (U,Zr)C (Carbide) Fuel Elements in the Nuclear Furnace 1 Test Reactor," LA-5398-MS, Los Alamos Scientific Laboratory, Los Alamos, New Mexico, 1973.

[3]Chen, Y.-S., Liu, J., Zhang, S., and Mallapragada, P., "An Integrated Tool for Launch Vehicle Base-Heating Analysis," Final Report, NAS8-00002, Engineering Sciences, Inc., Huntsville, AL, 2001.

[4]Chen. Y.-S., Zhang S., and Liu, J., "Stage Separation Performance Analysis Project," Final Report, H-34345D, Engineering Sciences, Inc., Huntsville, AL, 2002.

[5]Wang, T.-S., Chen, Y.-S., Liu, J., Myrabo, L.N., and Mead, F.B. Jr., "Advanced Performance Modeling of Experimental Laser Lightcraft," *Journal of Propulsion and Power,* **18**, 1129-1138 (2002).

[6]Wang, T.-S., "Multidimensional Unstructured-Grid Liquid Rocket Engine Nozzle Performance and Heat Transfer Analysis," AIAA Paper 2004-4016, 40th AIAA/ASME/SAE/ASEE Joint Propulsion Conference, Fort Lauderdale, Florida, 2004.

[7]Wang, T.-S., "Transient 3-D Analysis of Nozzle Side Load in Regeneratively Cooled Engines," AIAA Paper 2005-3942, 41st AIAA/ASME/SAE/ASEE Joint Propulsion Conference, Tucson, Arizona, 2005.

[8]Chen, Y.-S., and Kim, S. W., "Computation of Turbulent Flows Using an Extended k-ε Turbulence Closure Model," NASA CR-179204, 1987.

[9]Wang, T.-S., "Thermophysics Characterization of Kerosene Combustion," *Journal of Thermophysics and Heat Transfer*, **15**, 140-147 (2001).